Aerosol Science and Technology
Publication details, including instructions for authors and subscription information:
http://www.tandfonline.com/loi/uast20

Design and Calibration of a Counterflow Virtual Impactor for Sampling of Atmospheric Fog and Cloud Droplets

Kevin J. Noone [a], John A. Ogren [a], Jost Heintzenberg [a], Robert J. Charlson [b] & David S. Covert [c]

[a] Department of Meteorology, University of Stockholm, Arrhenius Laboratory, S-106 91, Stockholm, Sweden

[b] Department of Atmospheric Sciences, Univesity of Washington, Seatle, WA, 98195

[c] Department of Environmental Health, Univesity of Washington, Seatle, WA, 98195

Published online: 07 Jun 2007.

To cite this article: Kevin J. Noone, John A. Ogren, Jost Heintzenberg, Robert J. Charlson & David S. Covert (1988) Design and Calibration of a Counterflow Virtual Impactor for Sampling of Atmospheric Fog and Cloud Droplets, Aerosol Science and Technology, 8:3, 235-244, DOI: 10.1080/02786828808959186

To link to this article: http://dx.doi.org/10.1080/02786828808959186

Design and Calibration of a Counterflow Virtual Impactor for Sampling of Atmospheric Fog and Cloud Droplets

Kevin J. Noone, John A. Ogren, and Jost Heintzenberg
Department of Meteorology, University of Stockholm, Arrhenius Laboratory, S-106 91 Stockholm, Sweden

Robert J. Charlson
Department of Atmospheric Sciences, University of Washington, Seattle, WA 98195

David S. Covert
Department of Environmental Health, University of Washington, Seattle, WA 98195

An instrument is described that samples cloud droplets by removing them from the surrounding air and small unactivated particles through inertial impaction. The sampled droplets are then evaporated, leaving behind the material dissolved or suspended in the droplets as residue particles or gases. The instrument is capable of sampling droplets as a function of their size; it has an adjustable cut size in the range between about 9 and 30 μm in diameter, rejects droplets and particles smaller than the cut size, and captures droplets larger than the cut size. Details of the instrumental design and construction are discussed, as well as a relative calibration of the collection efficiency. Results from the calibration experiments indicate that the counterflow virtual impactor probe behaves in accordance with theoretical predictions using Stoke's number calculations. A complete description of the calibration methodology is presented.

NOMENCLATURE

B	Droplet mobility, $1/6\pi\eta r_d$(s/g)
C	Droplet molar concentration (moles/liter)
D	Inlet diameter (cm)
F_1	Return airflow rate to the probe (liters/min)
F_2	Sample stream flow rate (liters/min)
F_3	Excess flow rate out the probe tip (liters/min)
L	Distance from the probe tip to the internal stagnation plane (cm)
M	Solute mole weight (g/mole)
R	Probe radius (cm)
Re_d	Droplet Reynolds number, $2\rho_g r_d V_\infty/\eta$
V_∞	Free-stream air velocity (cm/s)
X	Porous tube length (cm)
f	Dimensionless stop distance correction factor, $\frac{3}{Re_d\kappa^{3/2}}\left[Re_d^{1/3}\kappa^{1/2} + \arctan\left(\frac{1}{Re_d^{1/3}\kappa^{1/2}}\right) + \frac{\pi}{2}\right]$
m_d	Droplet mass, $4\pi r_d^3\rho_d/3$ (g)
m_p	Particle mass, $4\pi r_p^3\rho_p/3$ (g)
r_d	Droplet radius (μm)
r_p	Particle radius (μm)
$y_{i,\text{data}}$	Optical particle counter response for the i^{th} size channel ($\mu m^3/cm^3$)
$y_{i,\text{ref}}$	Optical particle counter response for the i^{th} size class in a reference size distribution ($\mu m^3/cm^3$)

0278-6826/88/$3.50

y_k	Optical particle counter response in the k^{th} size channel used to determine α
α	Dimensionless normalization factor, $y_{k,\mathrm{ref}}/y_{k,\mathrm{data}}$
ϵ	Dimensionless collection efficiency $\alpha[y_{i,\mathrm{data}}/y_{i,\mathrm{ref}}]$
κ	Constant, 0.158
η	Air viscosity (g/cm*s)
ρ_d	Droplet density (g/cm^3)
ρ_g	Gas density (g/cm^3)
ρ_p	Particle density (g/cm^3)
£	Droplet stop distance, $V_\infty m_d Bf$ (cm)

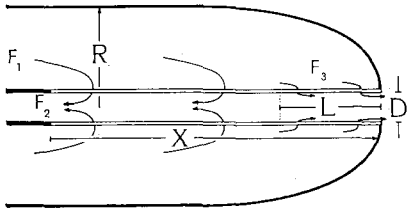

FIGURE 1. Parameters and nomenclature. Schematic diagram of the probe tip. X = porous tube length; L = distance to stagnation plane; R = probe radius; D = inlet diameter; F_1 = return airflow rate; F_2 = sample airflow rate; F_3 = excess airflow rate.

INTRODUCTION

In a collaborative effort between the University of Washington and the Department of Meteorology, Stockholm University (MISU), a counterflow virtual impactor (CVI) probe was developed that separates cloud or fog droplets from their surrounding gaseous and aerosol medium and evaporates them, leaving the material that was previously dissolved or suspended in the droplets as residue particles and the liquid water as water vapor. The initial version of the CVI described in Ogren et al. (1985) was designed as an aircraft sampling device. A second version of the device was designed to be both a calibration platform and a land-based cloud and fog droplet sampling instrument (Noone et al., 1986).

This paper describes the design of the device, a method of calibrating the CVI, and presents calibration results for the land-based instrument.

COUNTERFLOW VIRTUAL IMPACTOR: DESCRIPTION

The CVI probe is shown schematically in Figure 1, and its plumbing and test instrumentation are shown in Figure 2. The probe consists of two concentric tubes joined at the probe tip. The outer tube is solid, and the last 10 cm of the inner tube are porous. The probe is oriented such that the centerline of the concentric tubes is oriented parallel to the impaction velocity. Air that is filtered, dried, and heated is pumped to the probe tip through the annular space between the tubes with a flow rate F_1. This air passes through the walls of the porous tube. Part of the flow returns as a sample stream with a flow rate F_2, and part flows out the tip with a flow rate F_3. F_1 and F_2 are adjustable, and, because $F_3 = F_1 - F_2$, the flow out the tip is adjustable as well. Because the airflow through the walls of the porous tube is uniform (Noone, 1987), these flow rates define a distance from the probe tip to a stagnation plane within the porous tube where the velocity relative to the probe axis is zero. This distance can be expressed in terms of the flows as:

$$L = \left[\frac{(F_1 - F_2)}{F_1}\right] X = \left[\frac{F_3}{F_1}\right] X. \quad (1)$$

In addition to the flow velocity past the probe, two dimensions determine the minimum droplet size that the CVI probe will sample: the radius of the probe (R) and the distance from the probe tip to the interior stagnation plane (L). Approaching the probe, droplets follow the air streamlines until their inertia causes their trajectories to deviate from the streamlines. The magnitude of this deviation depends upon the particle

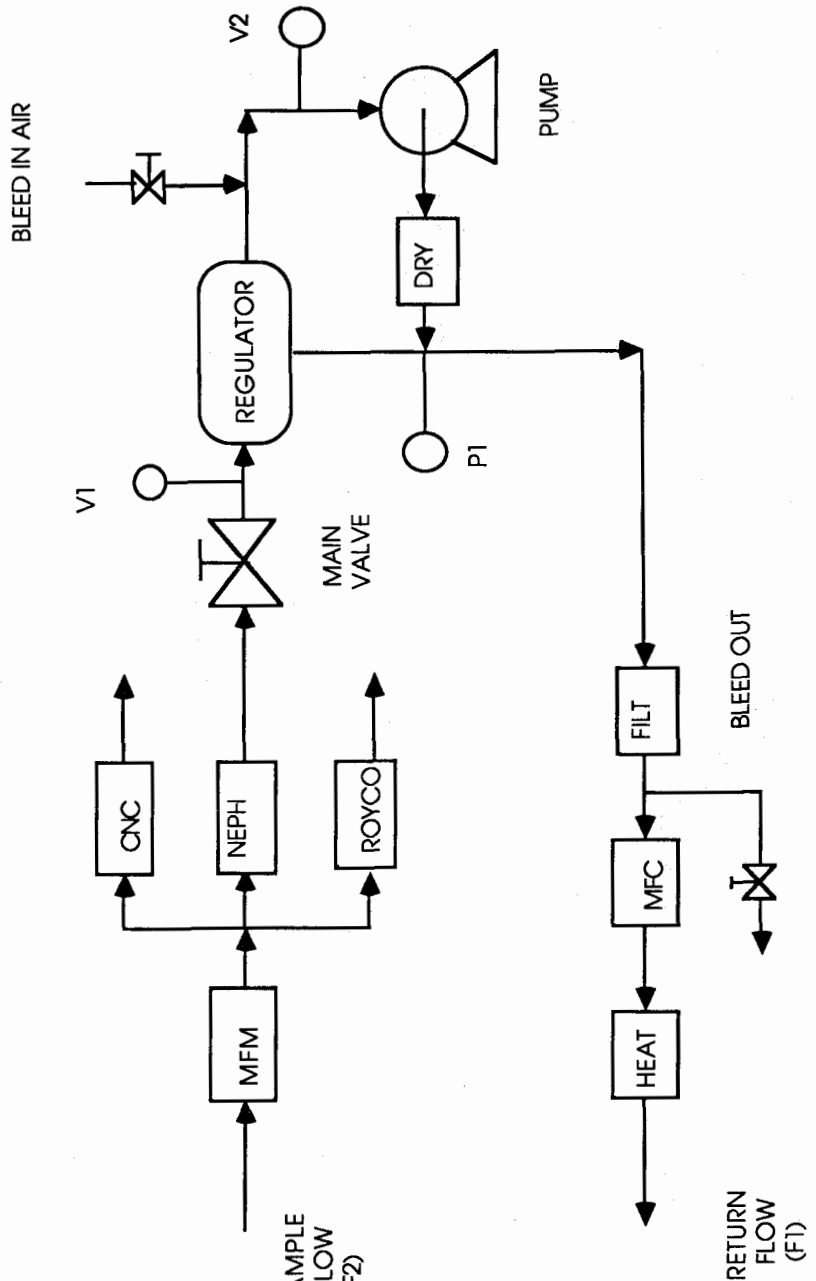

FIGURE 2. CVI plumbing diagram. The sample and return flows depicted in the diagram are connected to the probe/wind tunnel assembly. MFM and MFC denote mass flow meter and controller, respectively. The regulator and valve assembly dampens pulsations in the flow. Heat is supplied to the return flow via heating tape and a resistive heater.

mass and velocity. Droplets initially on a streamline close to the centerline of the probe, and with enough inertia to deviate sufficiently from the streamline, can enter the probe at its inlet aperture. To be sampled by the probe, the droplets must have enough inertia remaining to proceed through the impaction region of length L and into the sample flow. Droplets that are sampled by the probe must have stop distances greater than the sum of the distance to the stagnation plane (L) and some fraction of the probe radius (R).

The stop distance for supermicrometer droplets at Reynolds numbers between 0.5

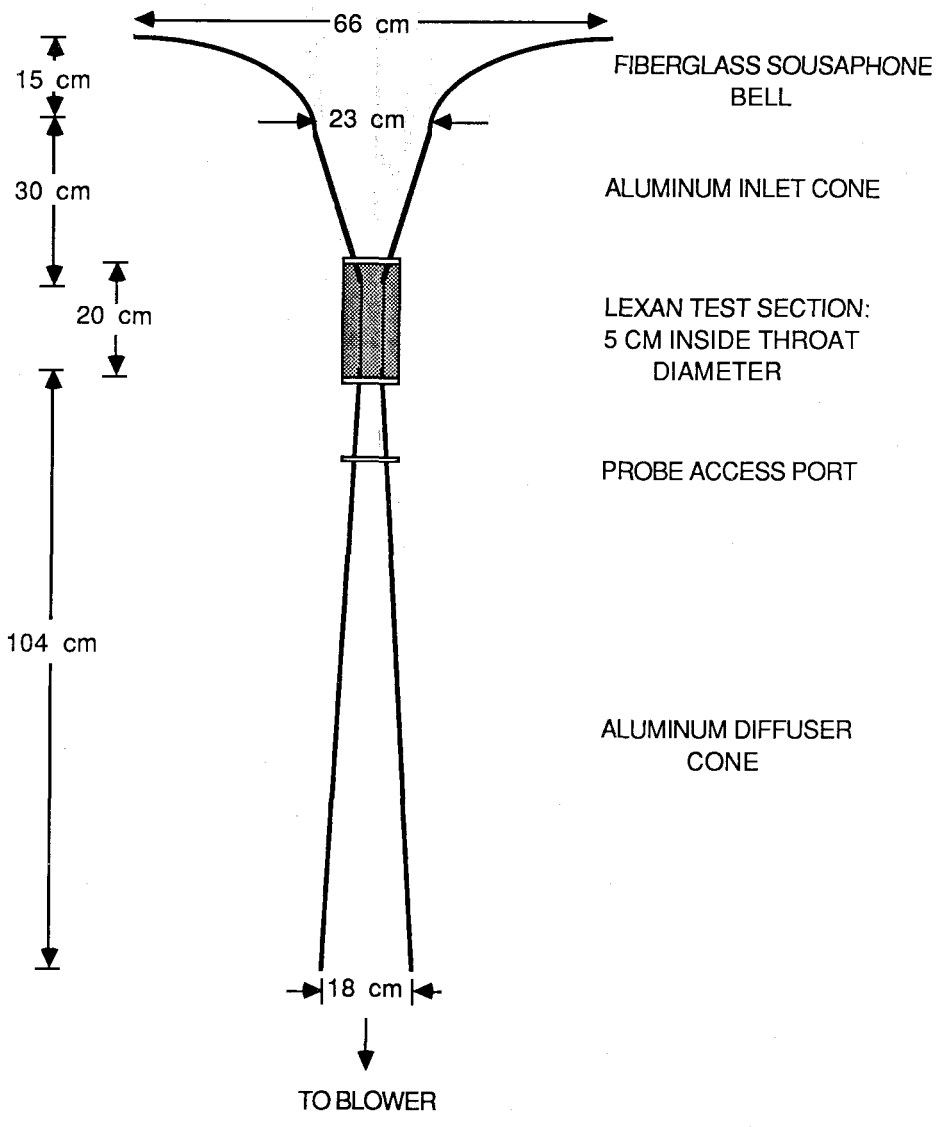

FIGURE 3. Schematic diagram of the wind tunnel. The wind tunnel is attached to a blower to provide the needed airflow. The CVI probe is located 5 cm downstream of the test section, on the centerline of the wind tunnel.

and 500 has been given by Serafini (1954) as:

$$\pounds = \left(\frac{r_d \rho_d}{3\rho_g \kappa^{3/2}}\right)\left[Re_d^{1/3}\kappa^{1/2} + \arctan\left(\frac{1}{Re_d^{1/3}\kappa^{1/2}}\right) + \frac{\pi}{2}\right]. \quad (2)$$

This expression can be simplified to express the stop distance as:

$$\pounds = V_\infty m_d B f, \quad (3)$$

where $V_\infty m_d B$ is the stop distance for Stokes flow, and f is a correction factor for flow outside the Stokes region. The droplet stop distance can then be used to estimate the cut size of the CVI. Because the flow field around and out of the probe has not been completely determined, we cannot calculate droplet trajectories entering the probe, and from them an exact cut size. We can, however, estimate a range of cut sizes for any given set of operating parameters. We know that in order to be sampled, the droplets must have stop distances greater than the range of distances L and $L + g(R)$, where $g(R)$ is some function of the probe radius. Although several investigators have modeled

FIGURE 4. CVI probe tip. The probe tip as shown here is connected to longer solid concentric tubes located on the centerline inside the wind tunnel. The sample and return lines are connected to the probe assembly through ports in the side of the wind tunnel at the base of the diffuser cone.

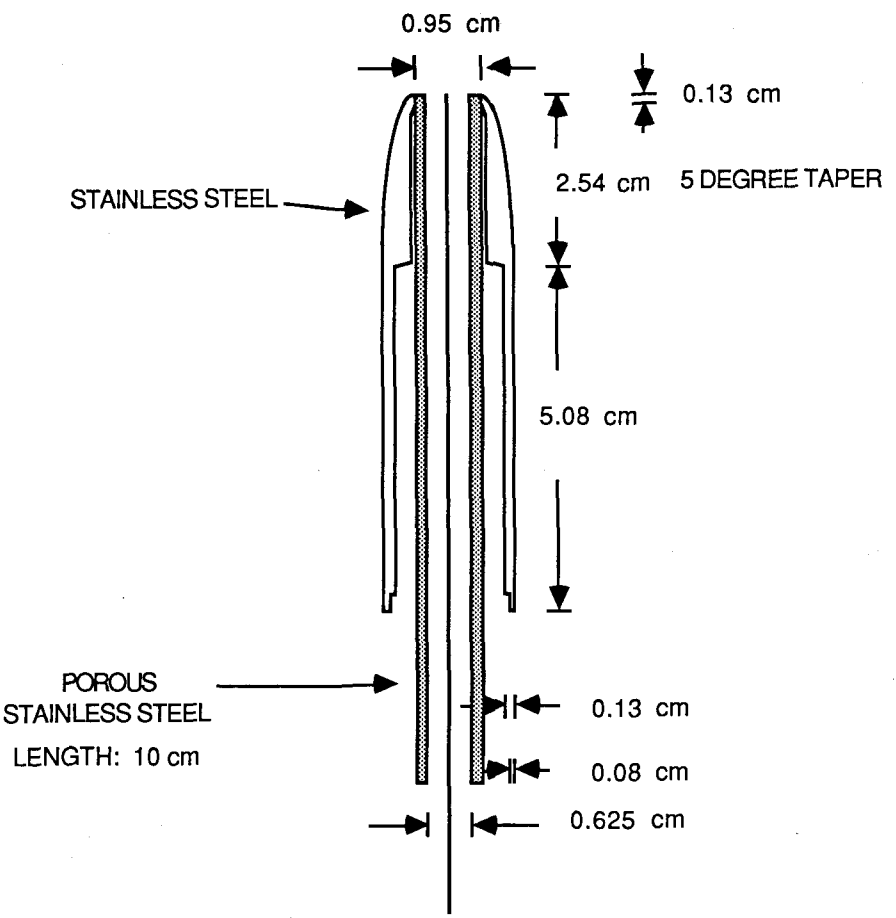

impaction of droplets on various geometrical shapes (Langmuir and Blodgett, 1946; Ranz and Wong, 1952; Dorsch et al., 1954; Banks and Kurowski, 1984), geometry and boundary flow conditions of the CVI are different than those used in the modeling investigations. We assume as a first approximation that $g(R) \approx R$. This allows us to calculate a range of droplet sizes within which the 50% collection efficiency (ϵ_{50}) should lie.

A small wind tunnel (depicted in Figure 3) was constructed to accelerate the droplets to approximately 100 m/s, providing the impaction velocity (V_∞) for the droplets. The inlet was constructed from a fiberglass sousaphone bell mated to an aluminum cone. The cone was attached to a cylindrical Lexan test section 10 cm long with a 5-cm i.d. The CVI probe was located 5 cm downstream of the test section in the center of the diffuser section of the tunnel. The end of the diffuser section was connected to a large fan (Universal Blower Model 8P1, United Blower Co., New York, NY) that provided the airflow through the wind tunnel. A diagram of the probe tip used in the calibration is provided in Figure 4.

FIGURE 5. Calibration assembly. A paint sprayer is used to generate droplets (10^{-3} M ammonium sulfate). The largest of the droplets are removed with a preimpactor, which also humidifies the air. The coated cardboard tube serves to constrain the droplet plume. Instrumentation is listed to illustrate the types of measurements possible with the CVI.

CALIBRATION

A diagram of the droplet production apparatus used to calibrate the land-based CVI is shown in Figure 5. A polydisperse droplet cloud was generated from a solution of

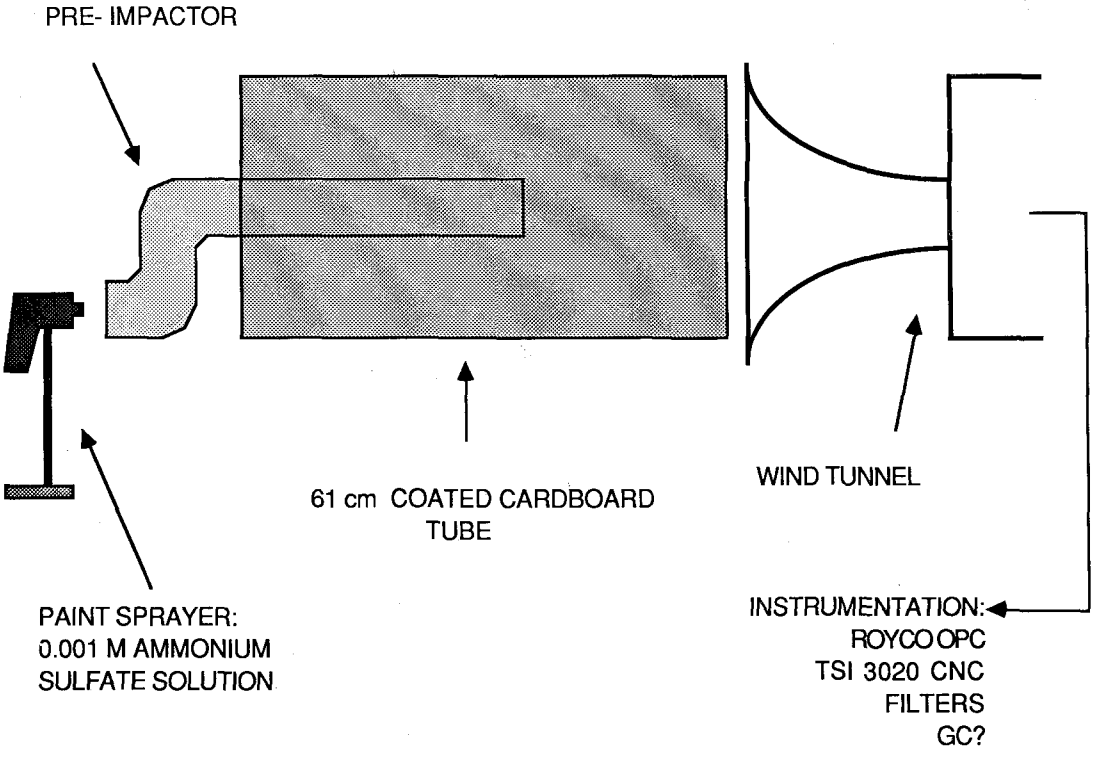

known composition (10^{-3} M ammonium sulfate) using a vibrating sprayer. The droplets were directed through two 90° elbows in 10-cm i.d. polycarbonate pipe to remove the largest droplets by impaction and sedimentation. Evaporation from the walls of these elbows and of the pipe also served to humidify the airstream containing the droplets. The droplets then passed through a short length of 10-cm polycarbonate tube and into the wind tunnel inlet. A 61-cm-diameter cylindrical form was placed in front of the inlet to prevent dispersal of the droplet plume. The transit time of the droplets from the generator to the probe was on the order of 2 s. The calibrations were done outside and at night when the relative humidity was high ($RH \geq 0.8$) to minimize droplet evaporation before impaction. From droplet evaporation calculations, the relative humidity of the airstream containing the droplets must be 0.99 or larger for evaporation to be negligible. Evaporation before impaction would cause the calculated droplet radius to be overestimated. Because there was no systematic overestimation of the cut size in the calibrations, droplet evaporation before impaction was not an important factor. Conversely, because the droplets and surrounding air are accelerated in the wind tunnel, the temperature in the test section will be lower than the ambient temperature, and it is possible for the air to become supersaturated. This supersaturation could lead to water vapor condensing on the droplets. Both evaporation and condensation effects would be most noticeable for the smaller droplets, and may help explain why the variance in the measured cut sizes decreased with increasing cut size.

Once in the wind tunnel, the droplets were accelerated to 100 m/s and impacted on the probe. The temperature in the sample line at steady state was 25–30°C, maintained with heating tape (100 W) on the return line just before it entered the wind tunnel, and a surface heater (HR5443, Minco Products Inc., Minneapolis, MN) on the probe just below the probe tip. Those droplets that entered the probe were evaporated, leaving the previously dissolved ammonium sulfate as dry particles. These particles were counted and sized using a calibrated optical particle counter (Royco OPC, Model 220). The OPC was calibrated by atomizing a solution of three different sizes of latex spheres, evaporating the associated water, and using the OPC to size the spheres. An adjustment was then made to account for the difference in the index of refraction between ammonium sulfate particles and latex spheres. Because the initial droplet concentration was known, it was possible to calculate the size of the droplets that entered the probe from the size of the dry particles in the sample stream:

$$r_d = \left[\frac{\rho_p}{10^{-3}CM}\right]^{1/3} r_p. \tag{4}$$

Through this relation, the size distribution of the droplets impacting on the probe could be calculated from the dry residue particle size distribution.

Initially, a reference distribution was obtained with the flows F_1 and F_2 set to give an L of 0 cm. The flows were then adjusted so that L increased in 1-cm increments up to a value of 8 cm. Collection efficiency curves were then obtained by dividing the size distributions into discrete intervals and comparing the number of droplets in each size interval in the distribution for a given L to the number of droplets in the same size interval in the reference distribution. A normalization factor is necessary to remove the effects of sampling time and possible changes in the droplet number concentration caused by dispersion of the droplet plume or small variations in the solution feed rate to the droplet generator. This normalization factor was obtained by first selecting a size interval in the droplet size distribution corresponding to droplets much larger than the estimated cut size of the probe. Assuming that these droplets were collected with an efficiency of 1, a normalization factor (α)

was defined by dividing the number of droplets in this size interval in the reference distribution by the number of droplets in this same size interval for each data distribution. This calculation is illustrated in Figure 6, where the graphs show the general shape of the residue particle volume size distribution. The difference in the area under the two curves would be proportional to the number of small droplets excluded when the cut size was increased. The collection efficiency for a particular value of L was then obtained through the relation:

$$\epsilon = \alpha\left[\frac{y_{i,\text{data}}}{y_{i,\text{ref}}}\right]. \tag{5}$$

Figure 7 is an example of an efficiency curve calculated in this manner. The sigmoidal shape of the curve can be seen; however, it is somewhat broader than typical efficiency curves for normal virtual impac-

FIGURE 6. Illustration of the efficiency calculation. The curves shown here reflect the general shape typical of calibration distributions. The calculation is performed by selecting a channel for normalization of the two distributions, then taking the ratio of the signals from the data and reference distributions in discrete intervals. The ratios are multiplied by the normalization factor to obtain the efficiency.

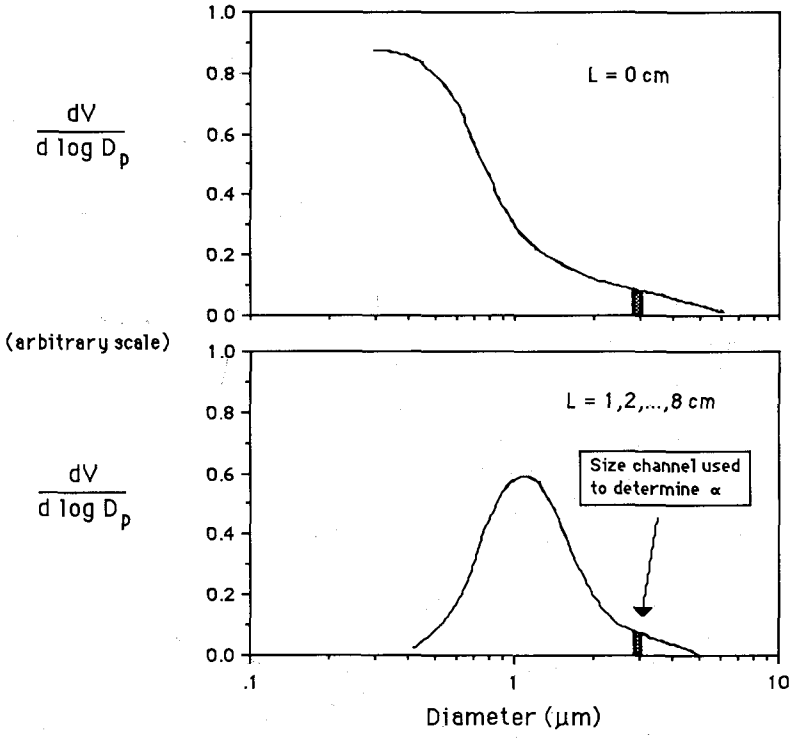

1) Define ε = 1 for a droplet diameter >> cut size

2) Let $\alpha = \dfrac{y_j\,(\text{ref})}{y_j\,(\text{data})}$ *for j = size where the efficiency is defined to be 1*

3) $\varepsilon = \alpha * \dfrac{y_i\,(\text{data})}{y_i\,(\text{ref})}$ i = number of size bin

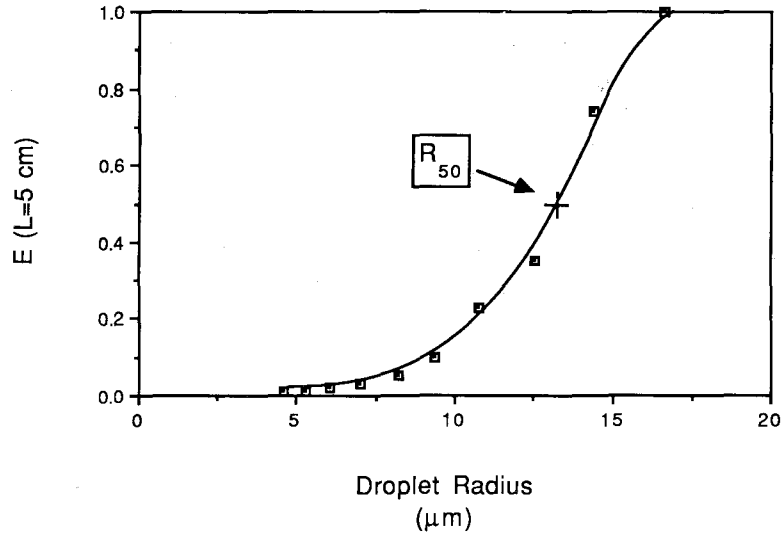

FIGURE 7. Typical measured efficiency curve. The sigmoidal shape characteristic of virtual impactors of the curve is apparent, although the curve is somewhat broader compared to curves for ordinary virtual impactors. The measured R_{50} is shown; the predicted value lies between 12 and 13 μm.

FIGURE 8. CVI calibration curve. The horizontal axis is the R_{50} from stop distance calculations. The horizontal bars reflect the range of droplet sizes having stop distances between L and $L+R$, with the plotted point being the median value. The vertical axis is the measured R_{50}, with the vertical bars being ± 1 SD around the mean, which is the plotted point.

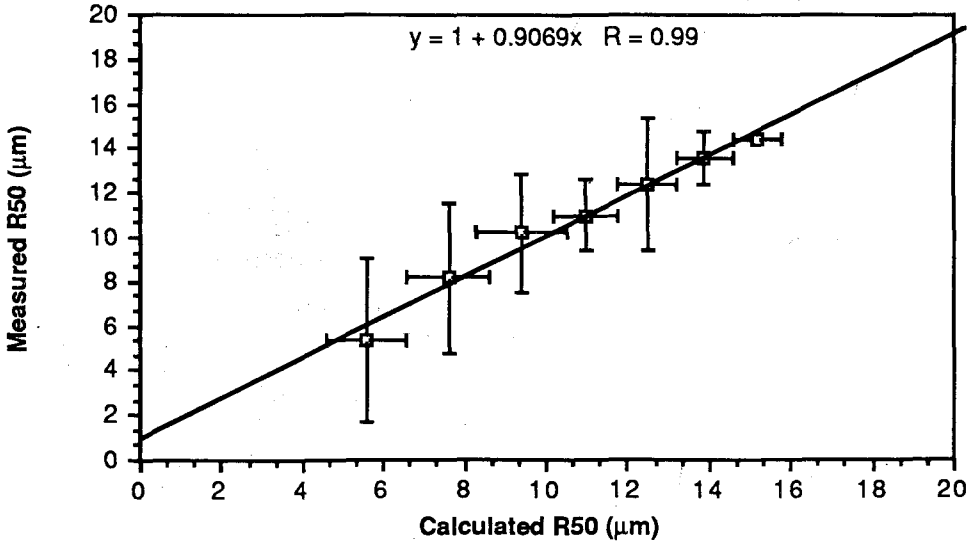

tors (Marple and Chien, 1980). There are several possible explanations for this broad shape. The flow field both inside and outside the CVI is more complicated than in an ordinary virtual impactor, making it difficult to determine precisely the actual distance a droplet travels before it crosses the internal stagnation plane and is sampled. Realistically, the internal stagnation plane may not be a plane, but rather a zone of finite width, introducing an uncertainty into the estimation of the length L. Once inside the probe, the droplets will begin to evaporate, changing their size. Due to the short residence time for these droplets inside the tip, we estimate the maximum decrease in droplet radius inside the porous tube to be around 10%. Because different sized droplets evaporate at different rates, it is possible that this small change in droplet radius could have some effect on the shape of the impaction efficiency curve.

Several runs were undertaken during the spring of 1986 to determine the repeatability of these calibrations. From the results of these runs, a calibration curve for the CVI was obtained and is shown in Figure 8. The horizontal axis is the theoretical 50% cut size, and the vertical axis is the measured 50% cut size. The horizontal bars around the data points reflect the range of droplet sizes having stop distances between L and $L + R$ for a V_∞ of 100 m/s, with the plotted point being midway between the two values. The vertical bars are ± 1 SD about the mean 50% collection efficiency in the calibration runs determined via the calculations described above. There are no vertical bars for the uppermost datum because only two measurements were made at this cut size. A linear regression of these data results in a line of slope 0.91 and a correlation coefficient of 0.99. The correlation coefficient indicates good agreement between theoretical and measured cut size values, whereas the slope is close to the ideal value of 1, indicating that the CVI functions as expected.

CONCLUSIONS

Calibration of the CVI indicates that it can be used to sample droplets or coarse aerosol particles as a function of their size. The size cut of the instrument can be adjusted by changing the airflow rates to and from the probe tip, and this cut size is found to be predictable from theoretical calculations.

This research has been funded through National Science Foundation grants ATM–8607377 and ATM–8318028.

REFERENCES

Banks, D. O., and Kurowski, G. J. (1984). *Aerosol Sci. Technol.* 3:317–326.

Dorsch, R. G., Brun, R. J., and Gregg, J. L. (1954). *NACA TN* 3099.

Langmuir, I., and Blodgett, K. B. (1946). *AAF TR* 5418.

Marple, V. A., and Chien, C. H. (1980). *Environ. Sci. Technol.* 14:976–984.

Noone, K. J. (1987). *Size Selective Cloud Drop Sampling Using a Counterflow Virtual Impactor: Design, Calibration, and Field Studies.* PhD Dissertation, University of Washington, Seattle, WA.

Noone, K. J., Charlson, R. J., Covert, D. S., Ogren, J. A., and Heintzenberg, J. (1987). Submitted to *J. Geophys. Res.*

Ogren, J. A., Heintzenberg, J., and Charlson, R. J. (1985). *Geophys. Res. Lett.* 12:121–124.

Ranz, W. E., and Wong, J. B. (1952). *Ind. Eng. Chem.* 44:1371–1381.

Serafini, J. S. (1954). *NACA TR* 1159.

Received 23 March 1987; revised and accepted 28 July 1987